Journal of Sound and Vibration (2001) **248**(1), 43–70
doi:10.1006/jsvi.2001.3696, available online at http://www.idealibrary.com on IDEAL®

PANEL ABSORBER

F. P. MECHEL

Landhausstrasse 12, *D*-71120-*Grafenau*, *Germany*

(*Received* 19 *September* 2000, *and in final form* 13 *March* 2001)

A plane wave is incident on a simply supported elastic plate covering a back volume; the arrangement is surrounded by a hard baffle wall. The plate may be porous with a flow friction resistance; the back volume may be filled either with air or with a porous material. The back volume may be bulk reacting (i.e., with sound propagation parallel to the plate) or locally reacting. Since this arrangement is of some importance in room acoustics, Cremer in his book about room acoustics [1] has presented an approximate analysis. However, Cremer's analysis uses a number of assumptions which make his solution, in his own estimate, unsuited for low frequencies, where, on the other hand, the arrangement mainly is applied. This paper presents a sound field description which uses modal analysis. It is applicable not only in the far field, but also near the absorber. Further, approximate solutions are derived, based on simplifying assumptions like Cremer has used. The modal analysis solution is of interest not only as a reference for approximations but also for practical applications, because the aspect of computing time becomes more and more unimportant (the 3D-plots presented below for the sound field were evaluated with modal analysis in about 6 s).

1. INTRODUCTION AND PROBLEM

Consider the object depicted in Figure 1. A simply supported one-dimensional elastic plate of thickness d and width $L = 2c$ is flush with a hard baffle wall. It covers a back volume with depth t. The medium in the volume is supposed to have the characteristic propagation constant Γ_a and wave impedance Z_a. If the medium is air without losses, $\Gamma_a = \mathrm{j}k_0$; $Z_a = Z_0$ with $k_0 = \omega/c_0$; $Z_0 = \rho_0 c_0$, ρ_0, c_0 being the density and sound speed of air. If the depth t of the volume is small, it is advisable to use for Γ_a, Z_a the characteristic values of a flat capillary. If the volume is filled with a porous material (not in tight mechanical contact with the plate) Γ_a, Z_a are the characteristic values of that material. The plate will be characterized in the present analysis by its partition impedance $Z_T = \Delta p/V$. The model of the one-dimensional plate agrees well with absorbers of this type applied in room acoustics where mostly long panels are used (i.e., one lateral dimension large compared to the other). The assumption of simple support of the panel borders also agrees best with the technical fixations among the classical supports (clamped, supported, free).

A plane wave p_e is incident normal to the z-axis with a polar angle Θ. The sound field in front of the absorber is composed as (the time factor $\mathrm{e}^{\mathrm{j}\omega t}$ is dropped)

$$\begin{aligned} p(x, y) &= p_e(x, y) + p_r(x, y) + p_s(x, y), \\ p_e(x, y) &= P_e \cdot \mathrm{e}^{-\mathrm{j}k_x x} \cdot \mathrm{e}^{-\mathrm{j}k_y y}, \\ p_r(x, y) &= P_e \cdot \mathrm{e}^{-\mathrm{j}k_x x} \cdot \mathrm{e}^{+\mathrm{j}k_y y}, \\ k_x &= k_0 \sin\Theta, \quad k_y = k_0 \cos\Theta \end{aligned} \tag{1}$$

where p_r is the incident wave after reflection at a hard plane in $y = 0$, and p_s is a scattered wave. The sum $p_e + p_r$ satisfies the boundary condition at the baffle wall, and has a zero

0022-460X/01/460043 + 28 $35.00/0

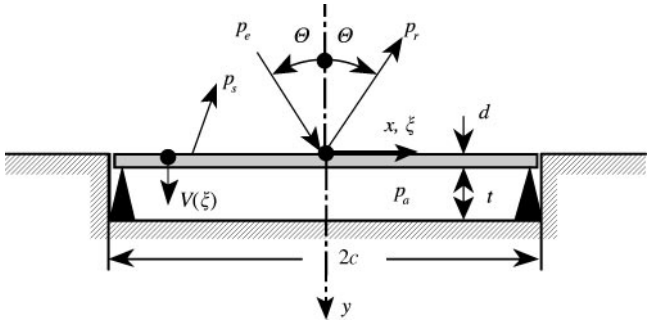

Figure 1. The object considered.

normal particle velocity at the plate also. Thus the normal particle velocity $v_{sy}(x, 0)$ of the scattered wave must agree with the plate velocity distribution $V(x)$ in the x range of the plate and must be zero outside that range.

Cremer [1] tried to solve the problem without detailed knowledge of p_s. In fact, it would be sufficient to know the plate velocity distribution $V(x)$, because with that the farfield angular distribution of p_s could be evaluated, see reference [2], and with this, the absorbed power could be computed. But the velocity distribution $V(x)$ in turn depends on p_s. Cremer tried to circumvent the problem of determination of p_s by some heuristic assumptions, and also gives only approximations for the sound field p_a in the volume. These approximations, in his own opinion, exclude the application of his solution at low frequencies.

In another approximation it would be sufficient to know the surface impedance $Z(x)$ of the plate surface; see reference [3]. This would be possible if the back volume would be locally reacting, e.g., by thin partitions in the volume or by a porous material filling with high flow resistivity. This assumption, however, would exclude the effects of a horizontal "pumping" of air in the volume by plate velocity profiles $V(x)$.

In order to avoid the suppression of possibly interesting effects by improper initial assumptions, a full field analysis will be performed below. The analysis of the present task is similar to the solution of the task of sound transmission through a simply supported plate in a baffle wall, which was described by Mechel [4]. Whereas the plate is loaded on its back side with $p_s(x)$ in the sound transmission problem, it is loaded here with the sound pressure $p_a(x)$ in the volume.

The next section will give the formulations for the component fields $p_e + p_r$, p_s, p_a, $V(x)$; the first two of these are formulated as sums of Mathieu functions; the sum coefficients for $p_e + p_r$ are explicitly known; the term factors for p_s must be determined from the boundary conditions. The volume field p_a is formulated as a sum of volume modes with unknown mode amplitudes; they also must be determined from the boundary conditions. Finally, the plate velocity profile $V(x)$ is formulated as the sum of modes of a simply supported (one dimensional) plate.

2. FORMULATIONS OF THE COMPONENT FIELDS

One begins with the formulation of $V(x)$, or $V(\xi)$ with $\xi = x/c$:

$$V(\xi) = \sum_{n \geqslant 1} V_n \cdot v_n(\xi),$$

$$v_n(\xi) = \begin{Bmatrix} \cos(n\pi\xi/2) = \cos(\gamma_n \xi), & n = 1, 3, 5, \ldots \\ \sin(n\pi\xi/2) = \sin(\gamma_n \xi), & n = 2, 4, 6, \ldots \end{Bmatrix}, \quad \gamma_n = n\pi/2. \tag{2}$$

The plate modes $v_n(\xi)$ are orthogonal to each other in $-1 \leqslant \xi \leqslant +1$ with the norms

$$N_{pn} = \int_{-1}^{1} v_n^2(\xi)\, \mathrm{d}\xi = 1. \tag{3}$$

Next, one formulates p_a. The wave and the momentum equations in the back volume have the forms

$$(\Delta - \Gamma_a^2)\, p_a = 0, \quad v_a = \frac{-1}{\Gamma_a Z_a} \operatorname{grad} p_a. \tag{4}$$

The formulation of p_a as a sum of volume modes,

$$p_a(x, y) = \sum_{k \geqslant 0} a_k \cdot p_{ak}(x) \cdot \cos(\kappa_k (y - t)), \tag{5}$$

$$\kappa_k c = \mathrm{j} \sqrt{(\Gamma_a c)^2 + \gamma_k^2}\,, \tag{6}$$

$$p_{ak}(\xi) = \begin{cases} \cos(k\pi\xi/2) = \cos(\gamma_k \xi), & k = 0, 2, 4, \ldots \\ \sin(k\pi\xi/2) = \sin(\gamma_k \xi), & k = 1, 3, 5, \ldots \end{cases}, \quad \gamma_k = k\pi/2, \tag{7}$$

satisfies the boundary conditions at the (hard) walls of the back volume. The volume modes are also orthogonal to each other in $-1 \leqslant \xi \leqslant +1$ with the norms

$$N_{ak} = \int_{-1}^{1} p_{ak}^2(\xi)\, \mathrm{d}\xi = \begin{cases} 2, k = 0 \\ 1, k > 0 \end{cases}. \tag{8}$$

The feature of $p_s(x, 0) = p_s(x)$ having a finite normal particle velocity $v_{sy}(x, 0)$ in $-c \leqslant x \leqslant +c$, and zero normal velocity outside, suggests the use of elliptic–hyperbolic cylinder co-ordinates (ρ, ϑ) for the formulation of that component field; see Figure 2.

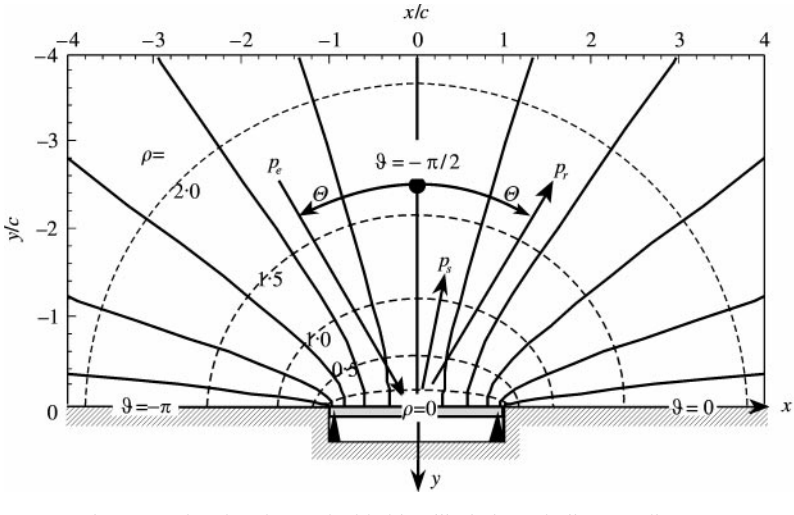

Figure 2. The absorber embedded in elliptic-hyperbolic co-ordinates.

These co-ordinates follow from the Cartesian co-ordinates (x, y) by the transformation $x = c \cdot \cosh \rho \cdot \cos \vartheta$, $y = c \cdot \sinh \rho \cdot \sin \vartheta$. $x = \pm c$ are the positions of the common foci of the ellipses and hyperbolic branches. At $\rho = 0$, $\xi = x/c = \cos \vartheta$.

The relations between vector components in elliptic–hyperbolic and Cartesian co-ordinates are (on the side shown in Figure 2)

$$v_\rho = v_x \frac{\sinh \rho \cdot \cos \vartheta}{\sqrt{\sinh^2 \rho + \sin^2 \vartheta}} + v_y \frac{\cosh \rho \cdot \sin \vartheta}{\sqrt{\sinh^2 \rho + \sin^2 \vartheta}} \xrightarrow[\rho \to 0]{} - v_y,$$

$$v_\vartheta = - v_x \frac{\cosh \rho \cdot \sin \vartheta}{\sqrt{\sinh^2 \rho + \sin^2 \vartheta}} + v_y \frac{\sinh \rho \cdot \cos \vartheta}{\sqrt{\sinh^2 \rho + \sin^2 \vartheta}} \xrightarrow[\rho \to 0]{} v_x. \tag{9a}$$

The gradient of a scalar function $p(\rho, \vartheta)$ has the form

$$\operatorname{grad} p = \frac{1}{c\sqrt{\cosh^2 \rho - \cos^2 \vartheta}} \left[\frac{\partial p}{\partial \rho} \mathbf{n}_\rho + \frac{\partial p}{\partial \vartheta} \mathbf{n}_\vartheta \right] \xrightarrow[\rho \to 0]{} \frac{1}{c \sin \vartheta} \left[\frac{\partial p}{\partial \rho} \mathbf{n}_\rho + \frac{\partial p}{\partial \vartheta} \mathbf{n}_\vartheta \right]. \tag{9b}$$

The wave equation in these co-ordinates is

$$\frac{\partial^2 p}{\partial \rho^2} + \frac{\partial^2 p}{\partial \vartheta^2} + (k_0 c)^2 (\cosh^2 \rho - \cos^2 \vartheta) \cdot p(\rho, \vartheta) = 0. \tag{9c}$$

It separates for $p(\rho, \vartheta) = U(\vartheta) \cdot W(\rho)$ into the two Mathieu differential equations (z is a general variable),

$$\frac{\mathrm{d}^2 U(z)}{\mathrm{d}z^2} + (b - 4q \cos^2 z)\, U(z) = 0,$$

$$\frac{\mathrm{d}^2 W(z)}{\mathrm{d}z^2} - (b - 4q \cosh^2 z)\, W(z) = 0, \tag{10}$$

with $q = (k_0 c)^2/4$ and b a separation constant. Solutions are the Mathieu functions (see references [4, 5] for these functions). A formulation of p_s which has the mentioned features for each term is

$$p_s(\rho, \vartheta) = 4 \sum_{m=0}^{\infty} D_m (-\mathrm{j})^m \operatorname{ce}_\mathrm{m}(\alpha) \cdot \operatorname{Hc}_\mathrm{m}^{(2)}(\rho) \cdot \operatorname{ce}_\mathrm{m}(\vartheta),$$

$$\alpha = \pi/2 - \Theta, \quad q = (k_0 c)^2/4. \tag{11}$$

The $\operatorname{ce}_\mathrm{m}(\vartheta)$ are "azimuthal Mathieu functions" which are even in ϑ at $\vartheta = 0$, and the $\operatorname{Hc}_\mathrm{m}^{(2)}(\rho) = \operatorname{Jc}_\mathrm{m}(\rho) - \mathrm{j} \cdot \operatorname{Yc}_\mathrm{m}(\rho)$ are associated "radial Mathieu functions", or "Mathieu–Hankel functions" of the second kind, which represent outward propagating waves and satisfy Sommerfeld's farfield condition. They are composed by the "Mathieu–Bessel" function $\operatorname{Jc}_\mathrm{m}(\rho)$ and the "Mathieu–Neumann" function $\operatorname{Yc}_\mathrm{m}(\rho)$ like the cylindrical Hankel function of the second kind. The Mathieu functions depend on the parameter q. The term amplitudes D_m are yet unknown. The azimuthal Mathieu functions are orthogonal to each other in $-\pi \leqslant \vartheta \leqslant 0$ with the norms

$$N_{sm} = \int_{-\pi}^{0} \operatorname{ce}_\mathrm{m}^2(\vartheta)\, \mathrm{d}\vartheta = \int_{0}^{\pi} \operatorname{ce}_\mathrm{m}^2(\vartheta)\, \mathrm{d}\vartheta = \frac{\pi}{2}. \tag{12}$$

One can note for later use that $\mathrm{ce_m}(\vartheta)$, $\mathrm{Jc_m}(\rho)$, $\mathrm{Yc_m}(\rho)$ are real functions, and $\mathrm{Jc'_m}(0) = 0$, $\mathrm{Hc_m^{\prime(2)}}(0) = -\mathrm{j}\cdot\mathrm{Yc'_m}(0)$ (where the primes indicate derivatives with respect to ρ). It will be important that the $\mathrm{ce_m}(\vartheta)$ are generated as a Fourier series

$$\mathrm{ce_m}(\vartheta) = \sum_{s=0}^{+\infty} A_{2s+p}\cdot\cos((2s+p)\vartheta), \quad m = 2r + p, \quad \left\{\begin{matrix} r = 0, 1, 2, \dots \\ p = 0, 1 \end{matrix}\right\}, \tag{13}$$

so the real Fourier coefficients A_{2s+p} are delivered by the computing program which generates the Mathieu function.

The sum $p_e + p_r$ can be expanded in Mathieu functions $\mathrm{ce_m}(\vartheta)$, $\mathrm{Jc_m}(\rho)$:

$$p_e(\rho, \vartheta) + p_r(\rho, \vartheta) = 4P_e \sum_{m=0}^{\infty} (-\mathrm{j})^m \mathrm{ce_m}(\alpha)\cdot\mathrm{Jc_m}(\rho)\cdot\mathrm{ce_m}(\vartheta) \tag{14}$$

(formulation (11) for p_s has inherited a formal similarity from this expansion).

With these formulations, the boundary conditions at the baffle wall and the walls of the back volume are satisfied, as well as Sommerfeld's condition. The formulations use functions which are orthogonal in $-1 \leqslant \xi \leqslant +1$. One is left with three sets of unknown amplitudes V_n, a_n, D_m and one still has three boundary conditions for their determination.

3. BOUNDARY CONDITIONS

The plate is supposed to be airtight. The boundary conditions at $y = 0$ and $-c \leqslant x \leqslant +c$, or $-1 \leqslant \xi \leqslant +1$, are

$$v_{sy}(\xi) = V(\xi), \quad v_{ay}(\xi) = V(\xi), \quad p_e(\xi) + p_r(\xi) + p_s(\xi) - p_a(\xi) = Z_T\cdot V(\xi). \tag{15}$$

The first condition follows from the fact that $p_e + p_r$ produce no normal particle velocity in the plane $y = 0$. The second condition is evident if one neglects the thickness d of the plate (more precisely, a new, shifted co-ordinate $y' = y + d$ could be defined in the back volume; the result would be the same). The right-hand side of the third condition still is "symbolic". It uses the partition impedance Z_T of the plate which is defined by $Z_T = (p_{front} - p_{back})/V$. The partition impedance, however, is defined only either for infinite, homogeneous plates or for finite plates if the driving pressure $(p_{front} - p_{back})$ has the profile of a plate mode. Then, Z_T represents the "modal partition impedance" Z_{Tn}.

In the present case of a simply supported plate, possibly with a loss factor η of the plate bending, the modal partition impedance is

$$\frac{Z_{Tn}}{Z_0} = 2\pi Z_m F\left[\eta F^2\left(\frac{\gamma_n}{k_0 c}\right)^4 + \mathrm{j}\left(1 - F^2\left(\frac{\gamma_n}{k_0 c}\right)^4\right)\right], \quad F = \frac{f}{f_{cr}}, \quad Z_m = \frac{f_{cr} d}{Z_0}\rho_p, \tag{16a}$$

with, respectively, ρ_p, f_{cr} the plate material density and the critical frequency of the plate (note that $f_{cr}d$ for thin plates is a material constant as well). Z_{Tn} immediately follows from the inhomogeneous bending wave equation. The case of an infinitely extended plate will be considered below for comparison; in that case the partition impedance Z_T is given by

$$\frac{Z_T}{Z_0} = 2\pi Z_m F[\eta F^2 \sin^4\Theta + \mathrm{j}(1 - F^2\sin^4\Theta)]. \tag{16b}$$

In order to give the third boundary condition a precise form, the fields on both sides are expanded in plate modes $v_n(\xi)$, and, with $Z_T \to Z_{Tn}$, it is required that the condition holds

term-wise. An intermediate form of the boundary condition is

$$p_e(\xi) + p_r(\xi) + p_s(\xi) - p_a(\xi) = \sum_{n \geqslant 1} V_n Z_{Tn} \cdot v_n(\xi). \tag{17}$$

With the expansion of the left-hand side in modes $v_n(\xi)$ one encounters the weak point of the present analysis. The sum over $v_n(\xi)$ with even n from equation (2) is a complete Fourier sine series for the anti-symmetrical part (in ξ) of the field; however the plate modes with odd n are not a complete set of orthogonal symmetrical functions because the constant function is missing. Therefore, an expansion of $p_e + p_r + p_s$ and of p_a in plate modes will create an unavoidable error at $\xi = \pm 1$, because both p_s and p_a will have relative maxima in these points. The following reasons suggest that it is worthwhile to proceed with the analysis, nevertheless. First, the range of the error near $\xi = \pm 1$ can be made arbitrarily small with sufficiently high values of n; second, the errors in $p_e + p_r + p_s$ and of p_a have the tendency to compensate each other; third, with a more acoustical reasoning, the errors $\Delta(p_e + p_r + p_s)$ and $\Delta(p_a)$ can be considered as additional fields which are restricted to a range near the support line of the plate, and there they will have only a minor influence on $V(\xi)$ because the plate is at rest in these points anyhow. These considerations show, that the expansion in $v_n(\xi)$ should only be used for boundary condition (17).

One can define the coupling coefficients

$$Q_{m,n} := \int_{-1}^{+1} \mathrm{ce_m}(\arccos \xi) \cdot v_n(\xi)\, \mathrm{d}\xi = \int_0^{\pi} \sin \vartheta \cdot \mathrm{ce_m}(\vartheta) \cdot v_n(\cos \vartheta)\, \mathrm{d}\vartheta, \tag{18a}$$

$$P_{m,k} := \int_{-1}^{+1} \mathrm{ce_m}(\arccos \xi) \cdot p_{ak}(\xi)\, \mathrm{d}\xi = \int_0^{\pi} \sin \vartheta \cdot \mathrm{ce_m}(\vartheta) \cdot p_{ak}(\cos \vartheta)\, \mathrm{d}\vartheta, \tag{18b}$$

$$S_{k,n} := \int_{-1}^{+1} p_{ak}(\xi) \cdot v_n(\xi)\, \mathrm{d}\xi. \tag{19}$$

Application on both sides of equation (17) of the integral

$$\int_{-1}^{+1} \cdots \cdot v_n(\xi)\, \mathrm{d}\xi, \quad n \geqslant 1,$$

gives

$$N_{pn} \frac{Z_{Tn}}{Z_0} \cdot Z_0 V_n$$

$$= 4 \sum_{m \geqslant 0} (-\mathrm{j})^m \mathrm{ce_m}(\alpha) \cdot Q_{m,n} \cdot [P_e \mathrm{Jc_m}(0) + D_m \mathrm{Hc_m^{(2)}}(0)] - \sum_{k \geqslant 0} a_k \cdot S_{k,n} \cdot \cos(\kappa_k t). \tag{20}$$

Next consider the boundary condition $v_{sy}(\xi) = V(\xi)$ with

$$v_{sy}(\rho = 0, \vartheta) = \frac{4}{k_0 c\, Z_0 \sin \vartheta} \sum_{m \geqslant 0} D_m (-\mathrm{j})^{m+1} \mathrm{ce_m}(\alpha) \cdot \mathrm{Hc_m'^{(2)}}(0) \cdot \mathrm{ce_m}(\vartheta) \tag{21}$$

(the prime indicates the derivative with respect to the argument ρ) and apply on both sides of $v_{sy}(\xi) = V(\xi)$ the integral

$$\int_0^{\pi} \cdots \cdot \sin \vartheta \cdot \mathrm{ce_m}(\vartheta)\, \mathrm{d}\vartheta,$$

with the result:

$$\frac{4}{k_0 c}(-\mathrm{j})^{m+1}\cdot N_{sm}\cdot \mathrm{ce_m}(\alpha)\cdot \mathrm{Hc_m^{\prime(2)}}(0)\cdot D_m = \sum_{n\geqslant 1} Z_0 V_n\cdot Q_{m,n},\quad m\geqslant 0. \tag{22}$$

Finally, consider the boundary condition $v_{ay}(\xi) = V(\xi)$ with

$$v_{ay}(\xi, y=0) = \frac{-1}{\Gamma_a Z_a}\sum_{k\geqslant 0} a_k\kappa_k\cdot p_{ak}(\xi)\cdot \sin(\kappa_k t) \tag{23}$$

and apply on both sides of the boundary condition the integral

$$\int_{-1}^{+1} \cdots \cdot p_{ak}(\xi)\,\mathrm{d}\xi,$$

with the result

$$a_k = \frac{-\Gamma_a Z_a}{\kappa_k\cdot N_{ak}\cdot \sin(\kappa_k t)}\sum_{n\geqslant 1} V_n\cdot S_{k,n},\quad k\geqslant 0. \tag{24}$$

Insertion of D_m from equation (22) and a_k from equation (24) into equation (20) leads to the linear, inhomogeneous system of equations for the amplitudes V_n ($v = 1, 2, 3, \ldots$):

$$\sum_{n\geqslant 1} Z_0 V_n\cdot\left\{\delta_{n.v}N_{pv} - \frac{k_0 c Z_0}{Z_{Tv}}\left[\frac{2\mathrm{j}}{\pi}\sum_{m\geqslant 0}\frac{\mathrm{Hc_m^{(2)}}(0)}{\mathrm{Hc_m^{\prime(2)}}(0)}\cdot Q_{m,v}Q_{m,n} + \frac{\Gamma_a Z_a}{k_0 Z_0}\sum_{k\geqslant 0}\frac{S_{k,v}\cdot S_{k,n}/N_{ak}}{\kappa_k c\cdot\tan(\kappa_k t)}\right]\right\}$$

$$= 4P_e\frac{Z_0}{Z_{Tv}}\sum_{m\geqslant 0}(-\mathrm{j})^m \mathrm{ce_m}(\alpha)\cdot Q_{m,v}\cdot \mathrm{Jc_m}(0), \tag{25}$$

with the Kronecker symbol $\delta_{n,v}$. After its solution, the amplitudes D_m, a_k follow from equations (22) and (24) respectively. It still remains to evaluate the coupling coefficients $S_{k,n}$, $Q_{m,n}$ for the computation of the component fields. A question is, whether the system of equations, which is infinite in principle, converges, so that it can be truncated. A sufficient criterion for convergence is the decrease or about constant magnitude of the main diagonal elements of the matrix with increasing v, further, a decrease of the matrix elements with increasing distance from the main diagonal, and finally a decrease of the right-hand side with increasing v. The first and last requirements are satisfied, because Z_{Tv}/Z_0, according to equation (16), increases as about v^4. The products of the coupling coefficients in the sum of the matrix coefficients decrease sufficiently with increasing k, m, n to satisfy the second requirement ($\cot(\kappa_k t)/(\kappa_k c)$ decreases as about $1/k$ for large k, and also the ratio of the Mathieu–Hankel function to its derivative at $\rho = 0$ decreases with increasing m).

4. COUPLING COEFFICIENTS

The coupling coefficients $S_{k,n}$,

$$S_{k,n} := \int_{-1}^{+1} p_{ak}(\xi)\cdot v_n(\xi)\,\mathrm{d}\xi,$$

$$p_{ak}(\xi) = \begin{Bmatrix} \cos(k\pi\xi/2) = \cos(\gamma_k\xi), & k = 0, 2, 4, \dots \\ \sin(k\pi\xi/2) = \sin(\gamma_k\xi), & k = 1, 3, 5, \dots \end{Bmatrix} \quad \gamma_k = k\pi/2,$$

$$v_n(\xi) = \begin{Bmatrix} \cos(n\pi\xi/2) = \cos(\gamma_n\xi), & n = 1, 3, 5, \dots \\ \sin(n\pi\xi/2) = \sin(\gamma_n\xi), & n = 2, 4, 6, \dots \end{Bmatrix}, \quad \gamma_n = n\pi/2, \tag{26}$$

are easily obtained. When indicating with a subscript e even numbers, and with a subscript o odd numbers, one gets

$$S_{k,n} = \begin{Bmatrix} 0, & k_e \ \& \ n_e \\ 0, & k_o \ \& \ n_o \\ \frac{2}{\pi}\left(\frac{(-1)^{(k_o - n_e - 1)/2}}{k_o - n_e} + \frac{(-1)^{(k_o + n_e - 1)/2}}{k_o + n_e}\right), & k_o \ \& \ n_e \\ \frac{2}{\pi}\left(\frac{(-1)^{(k_e - n_o - 1)/2}}{k_e - n_o} - \frac{(-1)^{(k_e + n_o - 1)/2}}{k_e + n_o}\right), & k_e \ \& \ n_o \end{Bmatrix}. \tag{27}$$

For the evaluation of the coupling coefficients $Q_{m,n}$ one uses the Fourier series representation of the $\mathrm{ce_m}(\vartheta)$ (see equation (13)):

$$Q_{m,n} := \int_{-1}^{+1} \mathrm{ce_m}(\arccos\xi)\cdot v_n(\xi)\,\mathrm{d}\xi = \int_0^{\pi} \sin\vartheta\cdot \mathrm{ce_m}(\vartheta)\cdot v_n(\cos\vartheta)\,\mathrm{d}\vartheta,$$

$$v_n(\xi) = \begin{Bmatrix} \cos(n\pi\xi/2) = \cos(\gamma_n\xi), & n = 1, 3, 5, \dots \\ \sin(n\pi\xi/2) = \sin(\gamma_n\xi), & n = 2, 4, 6, \dots \end{Bmatrix}, \quad \gamma_n = n\pi/2,$$

$$\mathrm{ce_m}(\vartheta) = \sum_{s=0}^{+\infty} A_{2s+p}\cdot\cos((2s+p)\vartheta), \quad m = 2r + p, \quad \begin{Bmatrix} r = 0, 1, 2, \dots \\ p = 0, 1 \end{Bmatrix}. \tag{28}$$

It follows from the fact that $\mathrm{ce_m}(\vartheta)$ is symmetrical in ϑ relative to $\vartheta = p/2$ if m is even, and odd if m is odd, that $Q_{m,n}$ has a non-zero value only for m_e & n_o and m_o & n_e (like the $S_{k,n}$).

One uses the second form for $Q_{m,n}$ and writes

$$Q_{m,n} = \sum_{s\geqslant 0} A_{2s+p}\cdot\int_{-1}^{+1} \sin\vartheta\cdot(\cos((2s+p)\vartheta)\cdot\begin{Bmatrix}\cos(\gamma_n\cos\vartheta), & n = \text{odd} \\ \sin(\gamma_n\cos\vartheta), & n = \text{even}\end{Bmatrix}\mathrm{d}\vartheta$$

$$= \sum_{s\geqslant 0} A_{2s+p}\cdot I_{s,n} \tag{29}$$

In $I_{s,n}$ one expands for $m = 2r$, even, i.e. $p = 0$ (see reference [6, equation 1.332.3]).

$$\sin\vartheta\cos(2s\vartheta) = \sin\vartheta + (1 - \delta_{0,s})\sum_{i=1}^{s}\frac{(-1)^i}{(2i)!}\cdot\sin^{2i+1}\vartheta\prod_{k=0}^{i-1}(4s^2 - 4k^2), \tag{30}$$

with the integrals (see reference [6, equation 3.715.21])

$$\int_0^{\pi}\sin^{2i+1}\vartheta\cos(\gamma_n\cos\vartheta)\,\mathrm{d}\vartheta = \sqrt{\frac{2\pi}{\gamma_n}}\left(\frac{2}{\gamma_n}\right)^i i!\cdot \mathrm{J}_{i+1/2}(\gamma_n) \tag{31}$$

leading to

$$Q_{2r,n} = \sqrt{\frac{2\pi}{\gamma_n}} \sum_{s \geqslant 0} A_{2s} \left[\mathrm{J}_{1/2}(\gamma_n) + (1 - \delta_{0,s}) \sum_{i=1}^{s} (-1)^i \frac{i!}{(2i)!} \left(\frac{2}{\gamma_n} \right)^i \cdot \mathrm{J}_{i+1/2}(\gamma_n) \prod_{k=0}^{i-1} (4s^2 - 4k^2) \right]. \tag{32}$$

For $m = 2r + 1$, odd, i.e., $p = 1$, one expands (see reference [6, equation 1.331.1])

$$\sin \vartheta \cos((2s+1)\vartheta) = \sin \vartheta \cos \vartheta \left[1 + (1 - \delta_{0,s}) \sum_{i=1}^{s} \frac{(-1)^i}{(2i)!} \prod_{k=1}^{i} ((2s+1)^2 - (2k-1)^2) \cdot \sin^{2i} \vartheta \right] \tag{33}$$

with the integrals (see Reference [6, equation 3.771.10]).

$$\int_0^{\pi} \sin \vartheta \cos \vartheta \sin^{2i} \vartheta \sin(\gamma_n \cos \vartheta) \, \mathrm{d}\vartheta = \int_{-1}^{+1} \xi (1 - \xi^2)^i \sin(\gamma_n \xi) \, \mathrm{d}\xi, \tag{34}$$

and gets

$$Q_{2r+1,n} = \sqrt{\frac{2\pi}{\gamma_n}} \sum_{s \geqslant 0} A_{2s+1} \times \left[\mathrm{J}_{3/2}(\gamma_n) + (1 - \delta_{0,s}) \sum_{i=1}^{s} (-1)^i \frac{i!}{(2i)!} \prod_{k=1}^{i} ((2s+1)^2 - (2k-1)^2) \left(\frac{2}{\gamma_n} \right)^i \cdot \mathrm{J}_{i+3/2}(\gamma_n) \right]. \tag{35}$$

The Bessel functions $\mathrm{J}_{k+1/2}(z)$ with half integer order can be evaluated from two starting values at high order with the known downward recursion for Bessel functions.

The coupling coefficients $P_{m,k}$ defined in equation (18b) must not be evaluated separately if one takes into account $p_{ak}(\xi) = v_{k+1}(\xi)$; thus $P_{m,k} = Q_{m,k+1}$.

An important question for the computing time is that for the upper limit m_{hi} of the order m of the Mathieu functions. From the pattern of $\mathrm{ce_m}(\vartheta)$ one can conclude that for a grazing wave with a number of $2c/(\lambda_0/2)$ pressure nodes along the plate, the order $m \approx 2c/(\lambda_0/2) = 2k_0 c/\pi$ will be the order with maximum contribution. So, one will set $m_{hi} = \mathrm{Int}(2k_0 c/\pi) + \Delta m$, with $\mathrm{Int}(x)$ the integer part of x and an increment Δm (≈ 2 to 4). The upper limit n_{hi} for the plate modes can be set to the same value $n_{hi} = m_{hi}$ (or somewhat higher).

5. SOUND ABSORPTION COEFFICIENT

The incident effective sound power (per unit length in the z direction) on the plate is

$$\Pi_e = \frac{c \cdot \cos \Theta}{Z_0} |P_e|^2. \tag{36}$$

The absorbed power (also per unit length) is (a star indicates the complex conjugate)

$$\Pi_a = \frac{c}{2} \mathrm{Re} \left\{ \int_{-1}^{+1} (p_e + p_r + p_s) \cdot v_{sy}^* \, \mathrm{d}\xi \right\}. \tag{37}$$

After insertion of

$$p_e + p_r + p_s = 4 \sum_{m \geqslant 0} (-\mathrm{j})^m \mathrm{ce_m}(\alpha)\,[P_e \cdot \mathrm{Jc_m}(0) + D_m \cdot \mathrm{Hc_m^{(2)}}(0)] \cdot \mathrm{ce_m}(\vartheta) \tag{38}$$

and v_{sy} from equation (21), integrals of the type

$$\int_{-1}^{+1} \frac{\mathrm{ce_m}(\vartheta) \cdot \mathrm{ce_\mu}(\vartheta)}{\sin \vartheta}\,\mathrm{d}\xi \xrightarrow[\xi = \cos \vartheta]{} \int_0^{\pi} \mathrm{ce_m}(\vartheta) \cdot \mathrm{ce_\mu}(\vartheta)\,\mathrm{d}\vartheta = \delta_{\mathrm{m},\mu} N_{sm} \tag{39}$$

will appear. With $N_{sm} = \pi/2$ and real $\mathrm{ce_m}(\alpha)$, $\mathrm{Jc_m}(0)$, $\mathrm{Yc_m}(0)$ and $\mathrm{Hc_m'^{(2)}}(0) = -\mathrm{j}\,\mathrm{Yc_m'}(0)$) one gets

$$\Pi_a = \frac{-4c\pi}{k_0 c Z_0} \sum_{m \geqslant 0} \mathrm{ce_m^2}(\alpha) \cdot \mathrm{Yc_m'}(0) \cdot \mathrm{Re}\{(P_e \cdot \mathrm{Jc_m}(0) + D_m \cdot \mathrm{Hc_m^{(2)}}(0)) \cdot D_{mj}^*\}. \tag{40}$$

The coefficients D_m are obtained from equation (22).

The sound absorption coefficient for oblique incidence finally is $\alpha(\Theta) = \Pi_a/\Pi_e$. The sound absorption coefficient $\alpha_{2-\mathrm{dif}}$ for two-dimensional diffuse sound incidence is obtained from

$$\alpha_{2\text{-dif}} = \int_0^{\pi/2} \alpha(\Theta) \cdot \cos \Theta\,\mathrm{d}\Theta. \tag{41}$$

If the surface impedance of the plate is not too low, this is a good approximation to the absorption coefficient for three-dimensional diffuse incidence, also.

6. BACK VOLUME LOCALLY REACTING

Some simplification is achieved if the back volume is supposed to be locally reacting, either by thin partition walls at small distances ($< \lambda_0/4$) or with a porous fill with sufficiently high flow resistivity Ξ ($\Xi \cdot t/Z_0 > 2$). An input impedance Z_b of the volume (at $y = 0$) then exists, $p_a(\xi) = Z_b \cdot v_{ay}(\xi)$, which is valid for all pressure profiles $p_a(\xi)$:

$$Z_b = Z_a \cdot \coth(\Gamma_a t). \tag{42}$$

Boundary conditions (15) then become

$$p_e(\xi) + p_r(\xi) + p_s(\xi) = \sum_{n \geqslant 1} V_n (Z_{Tn} + Z_b) \cdot v_n(\xi), \quad v_{sy}(\xi) = \sum_{n \geqslant 1} V_n \cdot v_n(\xi). \tag{43}$$

As in equations (38) and (39), the left-hand side of the first equation is expanded in plate modes, and the second equation leads to the amplitudes D_m of the scattered field terms, as in equations (21) and (22). The system of equations for the plate mode amplitudes V_n will be ($v = 1, 2, 3, \ldots$):

$$\sum_{n \geqslant 1} Z_0 V_n \cdot \left[\delta_{n,v} - \frac{2\mathrm{j}k_0 c}{\pi} \frac{Z_0}{Z_{Tv} + Z_b} \sum_{m \geqslant 0} Q_{m,v} \cdot Q_{m,n} \cdot \frac{\mathrm{Hc_m^{(2)}}(0)}{\mathrm{Hc_m'^{(2)}}(0)}\right]$$

$$= 4P_e \frac{Z_0}{Z_{Tv} + Z_b} \sum_{m \geqslant 0} (-\mathrm{j})^m \mathrm{ce_m}(\alpha) \cdot \mathrm{Jc}_m(0) \cdot Q_{m,v}. \tag{44}$$

The absorbed sound power again is taken from equation (40) with D_m from equation (22).

An alternative form for the absorbed sound power is obtained with equation (43):

$$\Pi_a = \frac{c}{2}\int_{-1}^{+1} \mathrm{Re}\left\{\sum_{n\geqslant 1} V_n(Z_{Tn}+Z_b)\cdot v_n(\xi)\cdot \sum_{n\geqslant 1} V_n^*\cdot v_n(\xi)\right\}\mathrm{d}\xi$$

$$= \frac{c}{2Z_0}\sum_{n\geqslant 1} N_{pn}\,\mathrm{Re}\left\{\frac{Z_{Tn}+Z_b}{Z_0}\right\}\cdot |Z_0 V_n|^2, \tag{45a}$$

$$\alpha(\Theta) = \frac{1}{2\sin\alpha}\sum_{n\geqslant 1}\mathrm{Re}\left\{\frac{Z_{Tn}+Z_b}{Z_0}\right\}\cdot |Z_0 V_n/P_e|^2. \tag{45b}$$

It is just the sum (with $N_{pn}=1$ for a simply supported plate) of the modal powers which the plate mode with amplitude V_n feeds into the impedance $Z_{Tn}+Z_b$.

Possibly, it was this simple relation which stimulated Cremer to evaluate the plate mode amplitudes V_n without explicit knowledge of the scattered field p_s. The fundamental "trick" in such approximations consists in the subdivision of the boundary value problem into two sub-tasks, and to make simplifying assumptions in the first sub-task. The next section will describe a similar method which, however, needs fewer assumptions than Cremer's solution.

7. APPROXIMATE SOLUTIONS

The main contribution to the needed numerical work in the above solution of the task comes from the evaluation of Mathieu functions for the scattered field p_s. This is the motivation to find a solution, even if it is only an approximation, without these functions. The principal step in such approximations is the subdivision of the boundary value problem into two sub-tasks. The first sub-task finds the plate mode amplitudes with the assumption, that $p_s(\xi)$ can be neglected compared to $p_e(\xi)+p_r(\xi)$. This sum is supposed to be the driving force for the plate motion. The assumption is plausible if the surface impedance of the plate is not too small. The second step then evaluates the absorbed power with the amplitudes V_n found in the first step.

If the back volume is supposed to be bulk reacting (i.e., possible sound propagation parallel to the plate) the boundary conditions in the mentioned approximation are

$$p_e(\xi)+p_r(\xi)-p_a(\xi) = 2P_e\cdot \mathrm{e}^{-\mathrm{j}k_x c\xi} - p_a(\xi) = \sum_{n\geqslant 1} V_n Z_{Tn}\cdot v_n(\xi),$$

$$v_{ay}(\xi) = \sum_{n\geqslant 1} V_n\cdot v_n(\xi), \tag{46}$$

where in the first equation, the left-hand side is supposed to be expanded in plate modes $v_n(\xi)$. It should be noted that this equation describes the excitation of the plate by a distributed force without radiation load on the side of excitation. Application on both sides of that equation of the integral

$$\int_{-1}^{+1} \cdots v_v(\xi)\,\mathrm{d}\xi, \quad v = 1, 2, 3, \ldots,$$

yields with $p_a(\xi)$ from equation (5) and the coupling coefficients $S_{k,n}$ from equation (26), together with the new coupling coefficients

$$R_n := \int_{-1}^{+1} \mathrm{e}^{-\mathrm{j}k_x c\xi} \cdot v_n(\xi)\, \mathrm{d}\xi = \left\{ \begin{array}{ll} \dfrac{4n\pi(-1)^n \cos(k_x c)}{(n\pi)^2 - 4(k_x c)^2}, & n = \text{odd} \\ \dfrac{-4\mathrm{j}n\pi(-1)^{n/2} \sin(k_x c)}{(n\pi)^2 - 4(k_x c)^2}, & n = \text{even} \end{array} \right\}, \tag{47}$$

the equations

$$V_v Z_{Tv} N_{pv} = 2P_e \cdot R_v - \sum_{k \geqslant 0} a_k \cdot S_{k,v} \cdot \cos(\kappa_k t) \tag{48}$$

and with the amplitudes a_k from equation (24) the system of equations for V_n ($v = 1, 2, 3, \ldots$)

$$\sum_{n \geqslant 1} V_n \cdot \left[\delta_{n,v} \cdot N_{pv} - \frac{\Gamma_a Z_a}{Z_{Tv}} \sum_{k \geqslant 0} \frac{S_{k,n} \cdot S_{k,v} \cdot \cot(\kappa_k t)}{\kappa_k \cdot N_{ak}} \right] = 2P_e \cdot \frac{R_v}{Z_{Tv}}. \tag{49}$$

If the back volume is locally reacting with the input impedance Z_b of equation (42), the only boundary condition of the first sub-task is

$$p_e(\xi) + p_r(\xi) = \sum_{n \geqslant 1} V_n (Z_{Tn} + Z_b) \cdot v_n(\xi). \tag{50}$$

Multiplication as before by $v_n(\xi)$ and integration immediately gives the V_n:

$$V_n = \frac{2P_e \cdot R_n}{(Z_{Tn} + Z_b)\, N_{pn}}. \tag{51}$$

The second sub-task determines the absorbed sound power, upon assuming that the plate velocity $V(\xi)$, expanded in $V_n \cdot v_n(\xi)$, is a given oscillation (i.e., again without consideration of a possible back reaction of radiation on the oscillation).

In a first variant of this step, one applies the product $(p_e(\xi) + p_r(\xi)) \cdot V^*(\xi)$ for the evaluation of the power which $(p_e(\xi) + p_r(\xi))$ feeds into the plate. So one makes the same error twice, because $(p_e(\xi) + p_r(\xi))$ is not the true exciting pressure. One gets

$$\Pi_{a1} = \frac{c}{2} \int_{-1}^{+1} \mathrm{Re} \left\{ (p_e(\xi) + p_r(\xi)) \cdot \sum_{n \geqslant 1} V_n^* \cdot v_n(\xi) \right\} \mathrm{d}\xi = P_e \cdot c \sum_{n \geqslant 1} \mathrm{Re}\{V_n^* \cdot R_n\}, \tag{52}$$

with R_n from equation (47) and V_n from either equation (49) or equation (51) for a bulk reacting or locally reacting back volume respectively.

In a second variant, one takes into account the sound pressure which the plate with the given velocity profile $V(\xi)$ radiates. One writes p_s for the radiated sound ($V(\xi)$ is counted positive in the direction oriented into the plate; thus the plate in fact is a sink for the energy of p_s). The knowledge of $V(\xi)$ is not sufficient to evaluate p_s near the plate, but its far field and power can be determined. The absorbed power is given by eqution (37), the integrand of which may be split into $(p_e(\xi) + p_r(\xi)) \cdot V^*(\xi) + p_s(\xi) \cdot V^*(\xi)$. The first term gives the power

contribution Π_{a1} of equation (52); the second term is the absorbed effective power Π_{as} due to p_s. This can be obtained by (see, e.g., reference [2])

$$\Pi_{as} = \frac{c}{2}\int_{-1}^{+1} \mathrm{Re}\{p_s(\xi)\cdot V^*(\xi)\}\,\mathrm{d}\xi = \frac{k_0 Z_0}{4\pi}\int_{-k_0}^{k_0} \frac{|\hat{v}(k_1)|^2}{\sqrt{k_0^2 - k_1^2}}\,\mathrm{d}k_1 = \frac{k_0 Z_0}{4\pi}\int_{-\pi/2}^{\pi/2} |\hat{v}(k_0\cos\psi)|^2\,\mathrm{d}\psi, \tag{53}$$

where $\hat{v}(k_1)$ is the wave number spectrum of $V(x)$, which follows by a Fourier transform ($L = 2c$ the plate width):

$$\hat{v}(k_1) = \int_{-\infty}^{+\infty} V(x)\cdot \mathrm{e}^{-\mathrm{j}k_1 x}\,\mathrm{d}x = \int_L V(x)\cdot \mathrm{e}^{-\mathrm{j}\,k_1 x}\,\mathrm{d}x = c\int_{-1}^{+1} V(\xi)\cdot \mathrm{e}^{-\mathrm{j}k_1 c\cdot\xi}\,\mathrm{d}\xi,$$

$$V(x) = \frac{1}{2\pi}\int_{-\infty}^{+\infty} \hat{v}(k_1)\cdot \mathrm{e}^{+\mathrm{j}k_1 x}\,\mathrm{d}k_1. \tag{54}$$

In the present application, $V(\xi)$ is the sum of terms $V_n\cdot v_n(\xi)$. The wave number spectrum $\hat{v}_n(k_1)$ of $v_n(\xi)$ is taken from equation (47) after multiplication with c and the substitution $k_x \to k_1$,

$$\hat{v}_n(k_1) = c\int_{-1}^{+1} \mathrm{e}^{-\mathrm{j}k_1 c\xi}\cdot v_n(\xi)\,\mathrm{d}\xi = \begin{cases} c\,\dfrac{4n\pi(-1)^n\cos(k_1 c)}{(n\pi)^2 - 4(k_1 c)^2}, & n = \text{odd} \\ c\,\dfrac{-4\mathrm{j}n\pi(-1)^{n/2}\sin(k_1 c)}{(n\pi)^2 - 4(k_1 c)^2}, & n = \text{even} \end{cases} \tag{55}$$

and the contribution to the absorbed power becomes

$$\Pi_{as} = \frac{k_0 Z_0}{4\pi}\int_{-\pi/2}^{\pi/2} \left|\sum_{n\geqslant 1} V_n\cdot \hat{v}_n(k_0\cos\psi)\right|^2 \mathrm{d}\psi. \tag{56}$$

The integral must be evaluated numerically. One cannot see in advance whether this correction to equation (52) is important or not.

The question as to why the scattered field in the second sub-task is determined in the far field is legitimate. (The reasons are the facts that the angular farfield distribution is proportional to the Fourier transform of the velocity $V(\xi)$ of the plate in a baffle wall, and that the radiated power can be evaluated from that distribution). One can next try a third variant of the second sub-task which somehow lies between the two previous variants. The first variant neglects the scattered field in the absorbed intensity $(p_e(\xi) + p_r(\xi))\cdot V^*(\xi)$; the second variant assumes a scattered field p_s and takes into account the fact that the plate is placed in a baffle wall; the third variant completes the absorbed intensity to $(p_e(\xi) + p_r(\xi) + p_s(\xi))\cdot V^*(\xi)$, but does not worry about possible scattering at the border lines between the plate and baffle wall.

One knows that $v_{sy}(\xi) = V(\xi) = \sum V_n\cdot v_n(\xi)$ at the plate surface. The scattered field is expanded in plate modes:

$$p_s(x, y) = \sum_{n\geqslant 1} d_n\cdot v_n(x)\cdot f_n(y). \tag{57}$$

A plausible form for $f_n(y)$ representing outgoing waves is $f_n(y) = \exp(\mathrm{j}\varepsilon_n y)$; the terms satisfy the wave equation and Sommerfeld's condition if $(\varepsilon_n c)^2 = (k_0 c)^2 - \gamma_n^2$; $\mathrm{Im}\{\varepsilon_n\} \leqslant 0$. From $v_{sy}(\xi) = V(\xi)$ one gets

$$d_n = -(k_0/\varepsilon_n)\,Z_0 V_n. \tag{58}$$

The absorbed power is

$$\Pi_a = \frac{c}{2}\int_{-1}^{+1} \mathrm{Re}\left\{(p_e(\xi) + p_r(\xi) + p_s(\xi))\cdot \sum_{n\geqslant 1} V_n^*\cdot v_n(\xi)\right\} \mathrm{d}\xi = \Pi_{a1} + \Pi_{as},$$

$$\Pi_{as} = \frac{c}{2}\int_{-1}^{+1} \mathrm{Re}\left\{\sum_{n\geqslant 1} d_n\cdot v_n(\xi)\cdot \sum_{n\geqslant 1} V_n^*\cdot v_n(\xi)\right\} \mathrm{d}\xi, \tag{59}$$

with Π_{a1} from equation (52), and the correction term

$$\Pi_{as} = \frac{-c}{2Z_0}\sum_{n\geqslant 1} \mathrm{Re}\left\{\frac{k_0}{\varepsilon_n}\right\}\cdot N_{pn}\cdot |Z_0 V_n|^2. \tag{60}$$

A very simple approximation, serving more for orientation than as approximation, is to assume the plate to be infinitely wide ($L\to\infty$). Then, the absorption coefficient $\alpha(\Theta)$ follows from the reflection factor R as $\alpha(\Theta) = 1 - |R|^2$ with

$$R = \frac{(Z_T + Z_b)\cdot\cos\Theta - Z_0}{(Z_T + Z_b)\cdot\cos\Theta + Z_0}, \tag{61}$$

where Z_T is the plate partition impedance from equation (16b) and Z_b is the input impedance of the back volume, which is given by equation (42) for a locally reacting volume, and by

$$\frac{Z_b}{Z_0} = \frac{\Gamma_{an} Z_{an}}{\Gamma_{an}\cos\theta_1}\cdot\coth(k_0 t\,\Gamma_{an}\cos\theta_1), \quad \Gamma_{an} = \Gamma_a/k_0,\ Z_{an} = Z_a/Z_0,$$

$$\Gamma_{an}\cos\theta_1 = \sqrt{\Gamma_{an}^2 + \sin^2\Theta} \tag{62}$$

for a bulk reacting volume.

8. NUMERICAL EXAMPLES

Some numerical examples will be shown (the plate still is supposed to be airtight). Curves of $\alpha(\Theta)$ over the frequency f will be shown first. Then, 3D-plots of the total sound field $|p/P_e|$ and of the scattered field $|p_s/P_e|$ will be presented at significant frequencies taken from $\alpha(\Theta)$.

One can begin with a bulk reacting back volume. Some parameters are kept constant in the examples. The plate is supposed to be a $d = 6$ mm thick plywood panel with a bending loss factor $\eta = 0{\cdot}02$ (it may include some losses at the fixation and by residual mechanical contacts with the porous material in the volume); the other material parameters of the plate are $\rho_p = 700\ \mathrm{kg/m^3}$, $f_{cr}\cdot d = 20\ \mathrm{Hz\cdot m}$. If the back volume with a depth $t = 10$ cm is filled, the filling is a glass fibre material with a given flow resistivity $\Xi = 2500\ \mathrm{Pa\ s/m^2}$. The used mode order limits are $n_{hi} = 10$ for the plate modes, $k_{hi} = 8$ for the volume modes, and $m_{hi} = 8$ for the Mathieu functions.

Figure 3 shows the sound absorption coefficient $\alpha(\Theta)$ over the frequency f; the angle of sound incidence is $\Theta = 45^\circ$; the panel is rather wide ($L = 2c$) with $c = 0{\cdot}5$ m. The full line is for the finite panel, the dashed curve is for the infinite panel. The comparison between both curves shows that the finite, supported panel has a marked low-frequency absorption (an absorption coefficient value above unity is regular for finite size absorbers with a high input

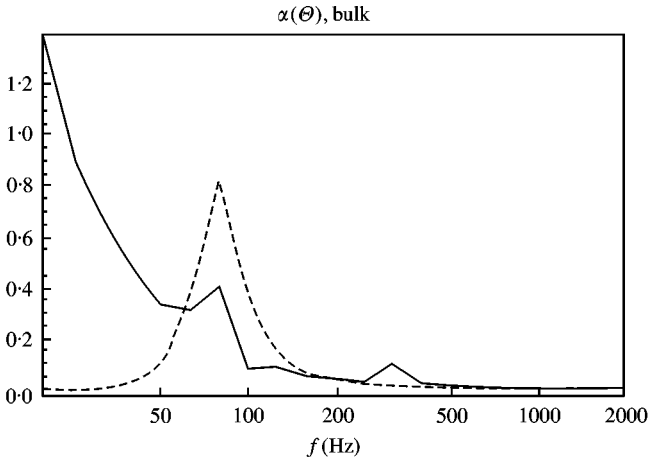

Figure 3. Sound absorption coefficient $\alpha(\Theta)$ for a wide plywood panel, simply supported (full line) and of infinite width (dashed).

admittance; it is a consequence of the so-called "border effect"; or in other words: the absorption cross-section is larger than the geometrical cross-section because of scattering at the borders). At the lowest resonance with $f \approx 20$ Hz the modes $n = 1$ and $m = 0$ are dominant; in the second resonance at $f \approx 80$ Hz the dominant plate mode is $n = 3$.

The magnitude of the total sound field at $f = 20$ Hz is shown in Figure 4(a). The plane wave in that diagram and similar further 3D-plots comes from the side of negative x/c values. The scattered wave p_s produces the difference of $|p(x,0)|$ from the value $|p_e(x,0) + p_r(x,0)| = 2$ not only in the range $-1 = x/c = +1$, but also well outside. The magnitude of the scattered field contained in Figure 4(a) is shown separately in Figure 4(b).

Similar field plots for the panel absorber of Figure 3, but now at frequency $f = 80$ Hz are contained in Figures 5(a) and (b). The field plot of |p| is jagged in the standing wave minimum, because the field was sampled along elliptic-hyperbolic co-ordinate lines. According to the now dominant plate mode $n = 3$ the field pattern at $y = 0$ shows more maxima and minima.

The next two diagrams, Figures 6(a) and 6(b) with $\alpha(\Theta)$ for $\Theta = 45^\circ$ and the same absorber as above, except the panel width has changed to $L = 2c = 0{\cdot}5$ m and $L = 0{\cdot}4$ m, respectively, illustrate that the achieved absorption is a matter of tuning of the parameters. This is not surprising, because the panel absorber has a number of possible resonance mechanisms: not only has the plate a number of resonances, but also the back volume (in its depth, with increase of the absorption, and its width, reducing the absorption), and coincidence of the panel vibration pattern $V(x)$ with the trace pattern of the incident wave also acts like a resonance.

Figure 7 shows the total sound pressure magnitude for the absorber of Figure 6(b) in the resonance at $f = 50$ Hz. A comparison with similar patterns for other parameters shows that the sound pressure profile also may seriously change with relatively small variations of the parameters.

In the next examples, the back volume is locally reacting. First, one considers the plywood panel with $c = 0{\cdot}5$ m, and the back volume with depth $t = 0{\cdot}15$ m filled with glass fibre material ($\Xi = 2500$ Pa s/m^2), which is supposed to be made locally reacting by thin partition walls. Figure 8 shows the absorption coefficients $\alpha(\Theta)$ both for the finite panel (full line) and for the infinite panel (dashed).

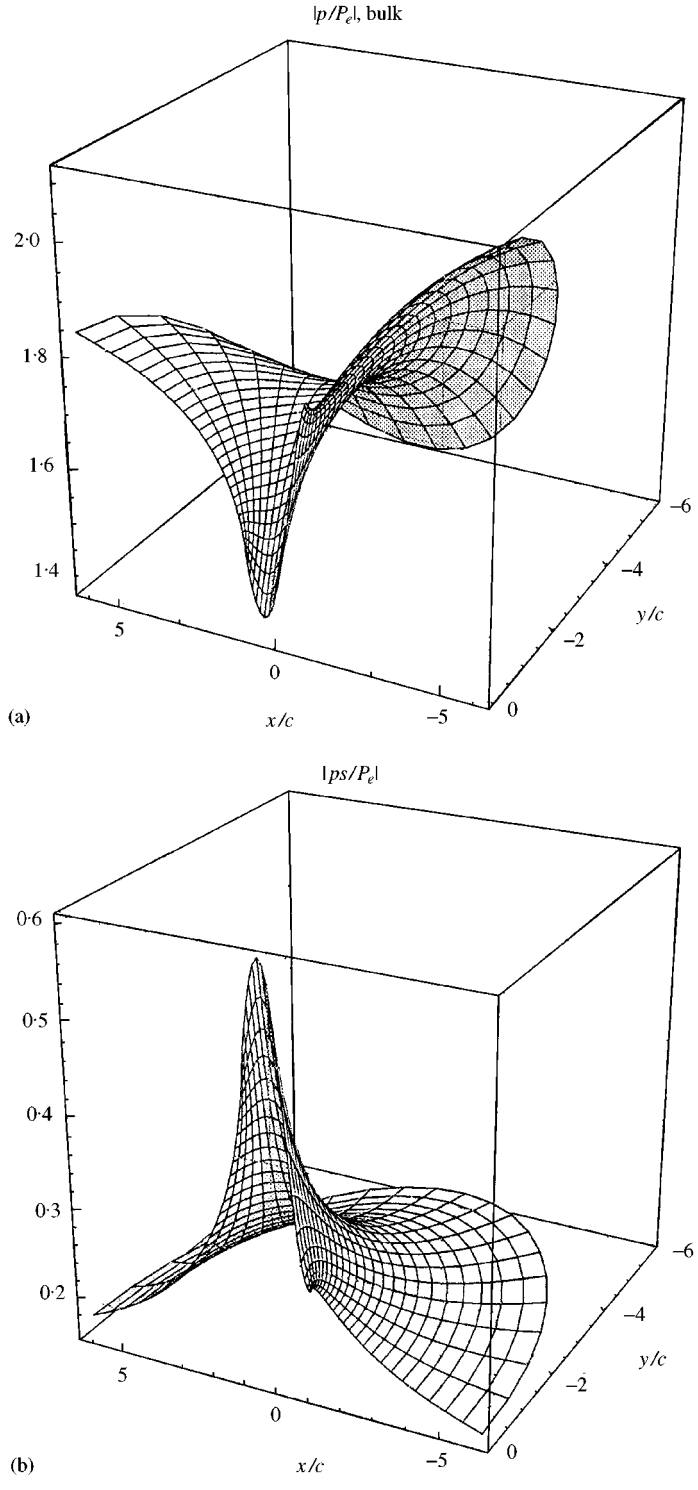

Figure 4. (a) Magnitude of the sound field at $f = 20$ Hz of Figure 3; (b) magnitude of the scattered field at $f = 20$ Hz of Figure 3.

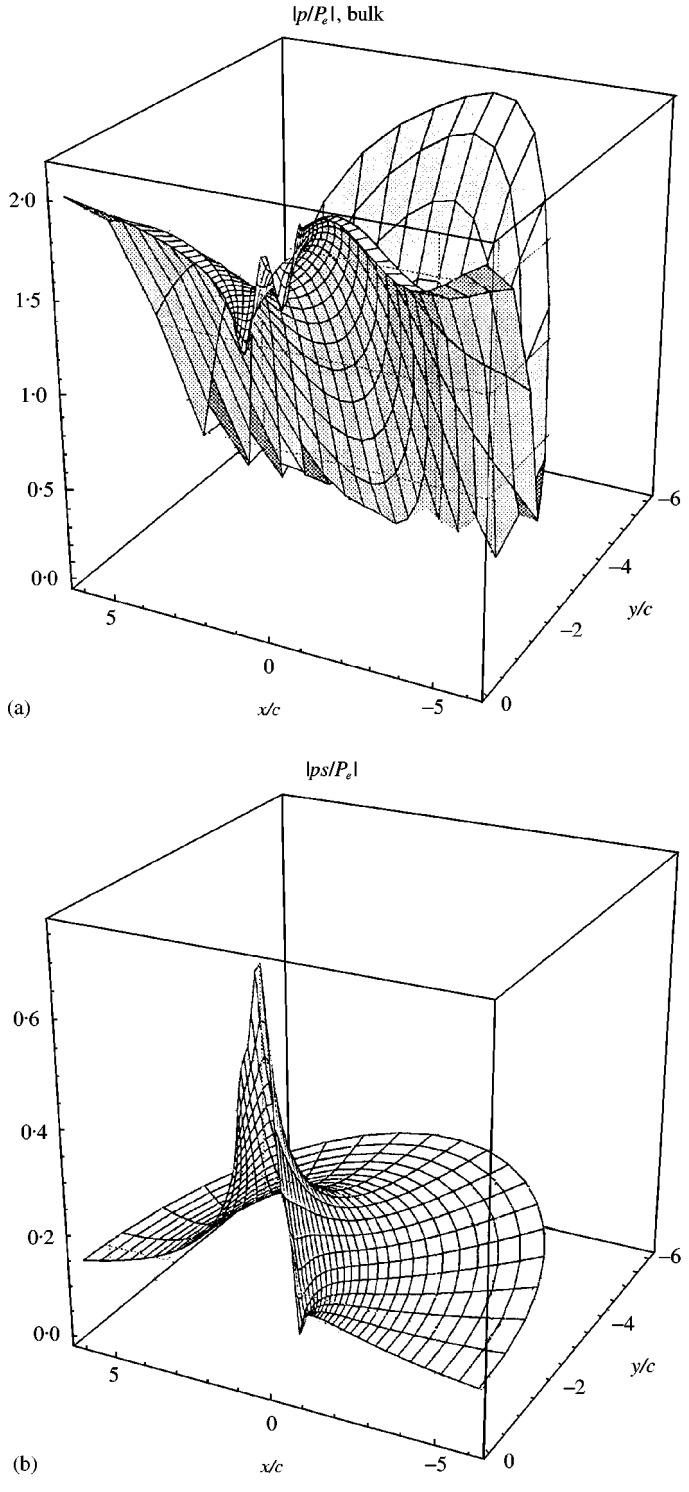

Figure 5. (a) Magnitude of the sound field at $f = 80$ Hz of Figure 3; (b) magnitude of the scattered field at $f = 80$ Hz of Figure 3.

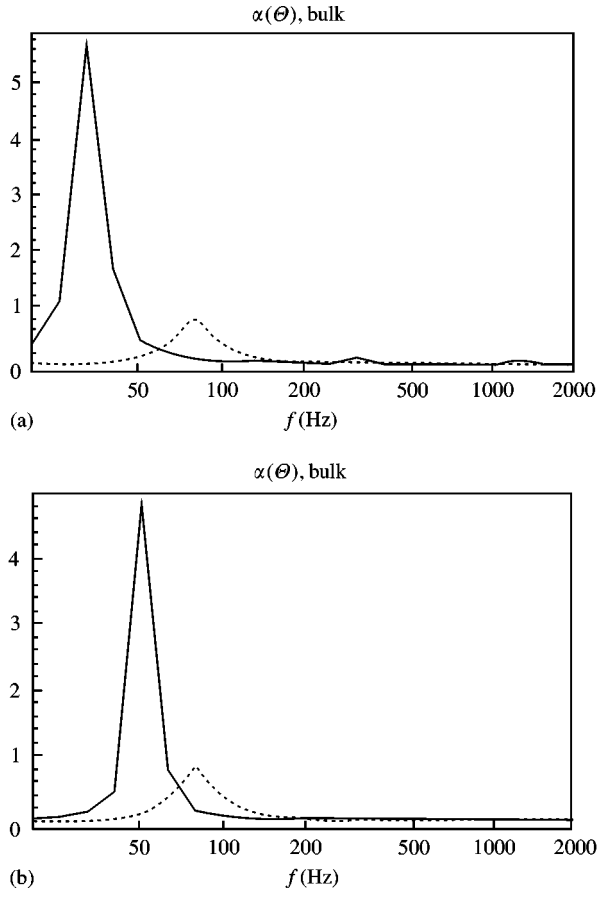

Figure 6. (a) Sound absorption coefficient $\alpha(\Theta)$ for a plywood panel absorber as in Figure 3, but with $c = 0{\cdot}25$ m; simply supported (full line) and of infinite width (dashed); (b) as (a), but with $c = 0{\cdot}20$ m.

The magnitude of the total field at $f = 80$ Hz for the panel absorber of Figure 8 is shown in Figure 9(a); of the scattered field in Figure 9(b). In the maximum at $f \approx 80$ Hz of Figure 8, the plate mode $n = 2$ and the Mathieu function $m = 2$ are clearly dominant (but are not the only existing modes).

Next, one can consider approximations for $\alpha(\Theta)$ with bulk reacting back volumes. Approximation "no. 1" uses equation (52), approximation "no. 2" applies the correction term of equation (56), approximation "no. 3" comes with the correction term from equation (60), and finally the approximation of the infinite plate evaluates $\alpha(\Theta) = 1 - |R|^2$ with R from the equations (61), (62). The curves for the different approximations are distinguished by different dashing; "no. 1" begins with a full line, and for increasing numbers, the dashes become shorter and shorter.

The example in Figure 10 belongs to the plywood panel with $c = 0{\cdot}25$ m and sound incidence under $\Theta = 45^\circ$ (see above for other parameters). It shows curves of $\alpha(\Theta)$ over frequency for the different approximations; it should be compared with Figure 6(a) from the modal analysis. According to Figure 10, the three approximations described in section 7 are about equivalent in the frame of agreement with the results from the modal analysis; that agreement is satisfying in the shown example, except in the resonance.

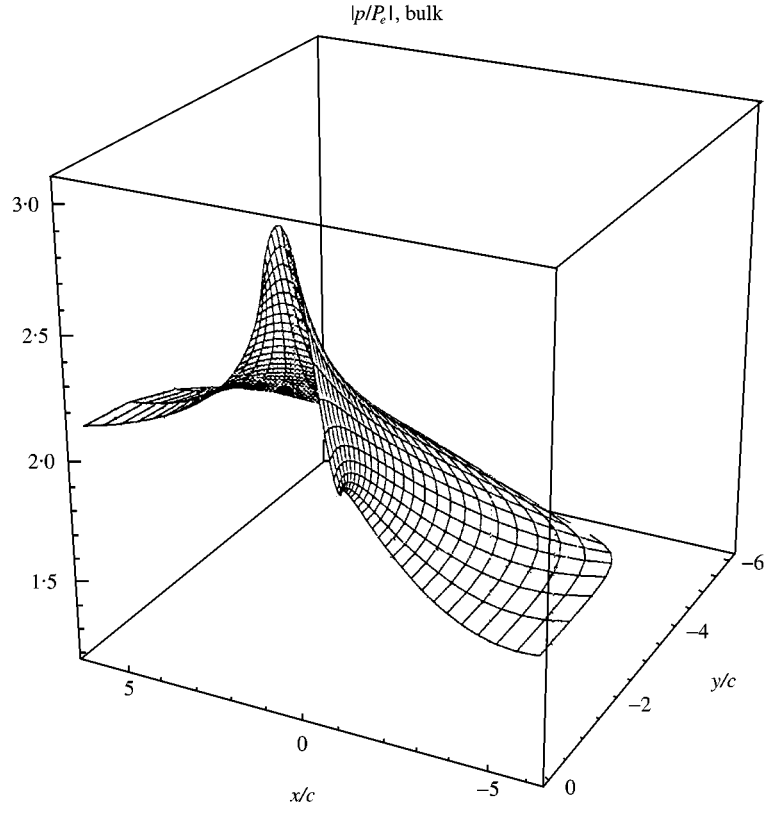

Figure 7. Magnitude of the sound field at $f = 50$ Hz of Figure 6(b).

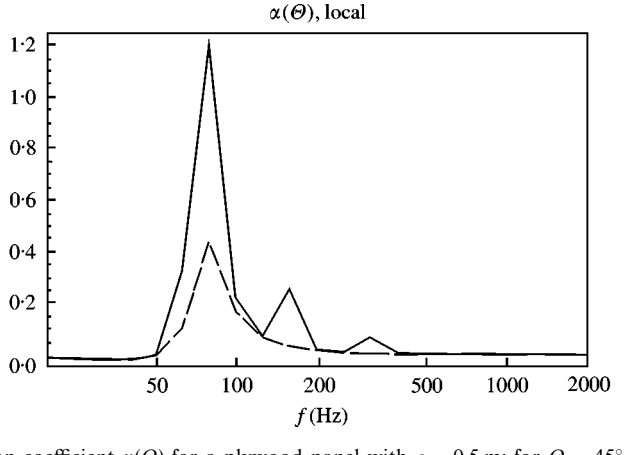

Figure 8. Absorption coefficient $\alpha(\Theta)$ for a plywood panel with $c = 0{\cdot}5$ m; for $\Theta = 45^\circ$. The back volume is locally reacting (full for finite panel, dashed for infinite panel).

9. ABSORBER WITH A POROUS PANEL

Panel absorbers as described above often are applied in room acoustics with some perforation of the panel. To make the perforation tractable in the analysis, it is supposed

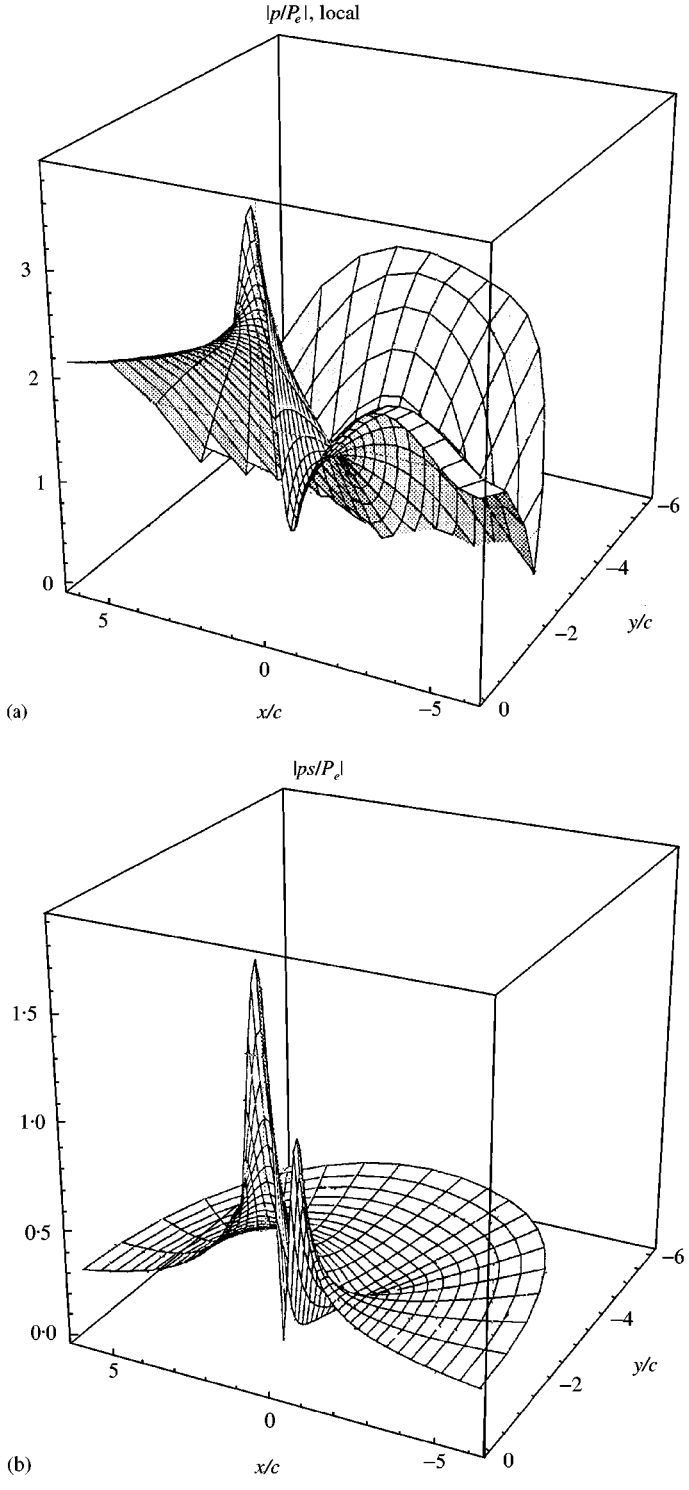

Figure 9. (a) Magnitude of the sound field at $f = 80$ Hz of Figure 8 for a panel absorber with $c = 0{\cdot}5$ m and locally reacting back volume; (b) magnitude of the scattered field at $f = 80$ Hz of Figure 8.

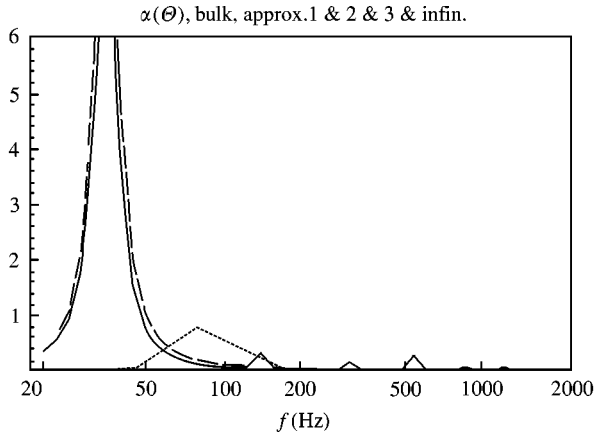

Figure 10. Approximations for $\alpha(\Theta)$ with a plywood panel, $c = 0{\cdot}25$ m, under sound incidence with $\Theta = 45°$; compare with Figure 6(a). Approximation no.1: full line; approximation no.2: long dash; approximation no.3: medium dash infinite plate: short dash.

that a "micro-structured" perforation is applied. This means that the diameter of the perforations and their distances are small compared with both the sound wavelength and the panel width. One further supposes a homogeneous distribution of the perforation over the panel (possibly except narrow border areas). In principle, a strip-wise perforation could be treated similarly (because one makes a full mode analysis); however the coupling coefficients would become integrals which would need numerical integration. The porosity of the panel is denoted by σ.

One first has to fix how the acoustic qualities of the perforation and the perforated panel have to be defined. The perforation changes the mechanical parameters, effective plate material density ρ_p and bending modulus B of the plate:

$$\rho_p \to \rho_p(1-\sigma), \quad B \to B\cdot(1-\sqrt{\sigma}), \quad f_{cr}d \to f_{cr}d\sqrt{\frac{1-\sigma}{1-\sqrt{\sigma}}}. \tag{63}$$

The indicated change in B is for square holes in a square array; it considers approximately the reduction of the solid plate material between the holes; more sophisticated relations can be derived for this and other geometries. The symbol Z_T is used here for the partition impedance of an equivalent tight plate, evaluated with these parameters and defined by $\Delta p = Z_T \cdot v_p$, where v_p is the velocity of this tight panel. The pores are characterized with an impedance $Z_r = Z_r' + \mathrm{j}\, Z_r''$ determined by $\Delta p = Z_r \cdot v_r$, where Δp is the pressure difference driving the average velocity v_r through the perforated plate at rest. Preferably, one determines Z_r' experimentally (because the technical roughness of hole walls and the effect of rounding of the hole corners are difficult to describe analytically; an exception could be straight, very fine holes for which the real part Z_r' can also be determined precisely from the theory of capillaries), and the imaginary part Z_r'' by evaluation from

$$\frac{Z_r''}{Z_0} = \frac{k_0 a}{\sigma}\left(\frac{d}{a} + \frac{\Delta\ell_e}{a} + \frac{\Delta\ell_i}{a}\right), \tag{64}$$

where a is any representative hole dimension (usually its radius), and $\Delta\ell_e$, $\Delta\ell_i$ are the exterior and interior end corrections respectively. One finds in reference [7] a number of end corrections for different hole shapes and arrays, where the important distinction is

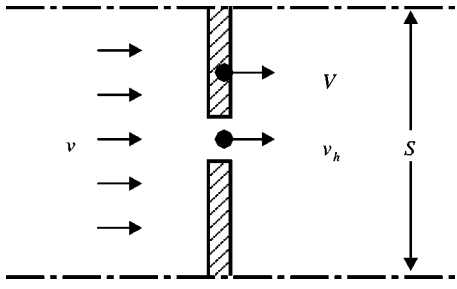

Figure 11. An element of the perforated panel.

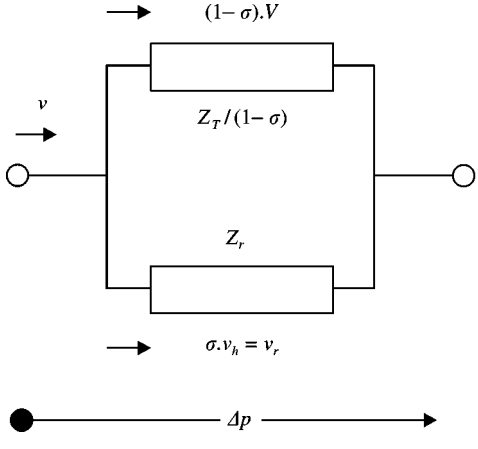

Figure 12. Equivalent network of the perforated panel.

made for the interior end correction whether the interior orifice ends in air or on a porous material. The reactance Z_r'' can generally be neglected for very narrow holes (and σ not too small) or for $\sigma \to 1$, or if the hole nearly occupies the whole area of an array element. Realizations of panel absorbers with interesting qualities can be constructed if Z_r is realized (in total or in part) by a thin resistive sheet (e.g., a fine wire mesh) on one side of the panel (usually the interior side).

The assumption of the micro structure of the perforation implies that the sound pressure distributions along the panel surfaces do not have significant ripples corresponding to the perforation pattern. The formulations of the component fields therefore remain as in section 2. For the determination of the unknown amplitudes a_k, D_m, V_n one needs three boundary conditions as in equation (15), but now modified for the parallel volume flow through the panel and the pores.

The sketch in Figure 11 indicates, in a representative area element S, the distribution of the velocities on the plate and in the holes. The average velocity is

$$v = (1-\sigma)\cdot V + \sigma \cdot v_h = (1-\sigma)\cdot V + v_r = (1-\sigma)\cdot V + \Delta p/Z_r. \tag{65}$$

The sketch in Figure 12 shows the equivalent network for the perforated panel.
The effective impedance is

$$Z_{eff} = \frac{Z_r \cdot Z_T/(1-\sigma)}{Z_r \cdot Z_T + (1-\sigma)} \tag{66}$$

and the first boundary condition becomes

$$\Delta p = Z_{eff} \cdot v = \frac{Z_r \cdot Z_T/(1-\sigma)}{Z_r + Z_T/(1-\sigma)} [(1-\sigma) \cdot V + \Delta p/Z_r], \tag{67a}$$

or with a transformation, if $\sigma \neq 1$,

$$\Delta p \frac{Z_r}{Z_r + Z_T/(1-\sigma)} = \frac{Z_r \cdot Z_T}{Z_r + Z_T/(1-\sigma)} \cdot V. \tag{67b}$$

This corresponds to the boundary condition with airtight plates if one uses the effective plate partition impedance

$$Z_{Teff} = \frac{Z_r \cdot Z_T}{Z_r + Z_T/(1-\sigma)}. \tag{68}$$

From equation (67a) one finds the expected limits

$$\Delta p \xrightarrow[\substack{Z_r \to \infty}]{\sigma \to 0} Z_T \cdot V, \quad \Delta p \xrightarrow[\sigma \to 1]{} Z_r \cdot v_r,$$

$$\Delta p \xrightarrow[\substack{v_r \to 0}]{Z_r \to \infty} Z_T \cdot V, \quad \Delta p \xrightarrow[\substack{v_r \to \infty}]{Z_r \to 0} Z_r \cdot v_r. \tag{69}$$

In these relations, $\Delta p = p_e + p_r + p_s - p_a$.

The other boundary conditions of matching velocities become

$$v = (1-\sigma) \cdot V + \Delta p/Z_r \overset{!}{=} \begin{Bmatrix} v_{sy} \\ v_{ay} \end{Bmatrix}. \tag{70}$$

The derivations from equations (66) to (68) tacitly contain an assumption: it is supposed that the friction force on the plate can be neglected compared to the driving force from Δp. This assumption is plausible if the holes of the perforation are sufficiently wide (say a few millimetres) and the porosity is not too high. In the realization with the wire gauze at an orifice, it is supposed that the gauze either does not vibrate (due to its surface mass density) or it is not force-locking with the panel. But for large porosity values with narrow pores or with a force locking, vibrating wire mesh, the friction exerts an additional force ΔF_r on the panel, if the relative velocity $v_h - V \neq 0$. The driving force on the panel in a section S then becomes

$$\Delta F = \Delta F_p + \Delta F_r = Z_T \cdot V S_p + \sigma Z_r' \cdot (v_h - V) S_h, \tag{71}$$

or after division with the plate area S_p,

$$\Delta p = \left[Z_T + Z_r' \frac{\sigma}{1-\sigma} \left(\frac{v_r}{V} - \sigma \right) \right] \cdot V = \left[Z_T + Z_r' \frac{\sigma}{1-\sigma} \left(\frac{\Delta p/Z_r}{\Delta p/Z_T} - \sigma \right) \right] \cdot V$$

$$= \left[Z_T + Z_r' \frac{\sigma}{1-\sigma} \left(\frac{Z_T}{Z_r} - \sigma \right) \right] \cdot V. \tag{72}$$

The expression in the last brackets replaces Z_T in equations (66)–(70) if friction force coupling must be taken into account.

After these preparations, one has the boundary conditions

$$\Delta p = \sum_{n \geqslant 1} Z_{Teffn} \cdot V_n \cdot v_n(\xi), \tag{73a}$$

$$v_{sy} = (1 - \sigma) \cdot V + \Delta p / Z_r, \quad v_{ay} = (1 - \sigma) \cdot V + \Delta p / Z_r. \tag{73b, c}$$

A combination of equation (73a) with equation (73b) and with equation (73c) gives

$$v_{sy} = \sum_{n \geqslant 1} V_n \cdot v_n(\xi) \left[(1 - \sigma) + \frac{Z_{Teffn}}{Z_r} \right], \quad v_{ay} = \sum_{n \geqslant 1} V_n \cdot v_n(\xi) \left[(1 - \sigma) + \frac{Z_{Teffn}}{Z_r} \right], \tag{74a, b}$$

with (see equations (21) and (23)),

$$v_{sy}(\rho = 0, \vartheta) = \frac{-4}{k_0 c Z_0 \sin \vartheta} \sum_{m \geqslant 0} D_m (-\mathrm{j})^m \mathrm{ce_m}(\alpha) \cdot \mathrm{Yc'_m}(0) \cdot \mathrm{ce_m}(\vartheta), \tag{75a}$$

$$v_{ay}(\xi, y = 0) = \frac{-1}{\Gamma_a Z_a} \sum_{k \geqslant 0} a_k \kappa_k \cdot p_{ak}(\xi) \cdot \sin(\kappa_k t). \tag{75b}$$

Performing on both sides of equation (74a) the integral

$$\int_0^\pi \cdots \sin \vartheta \cdot \mathrm{ce_m}(\vartheta) \, \mathrm{d}\vartheta$$

gives

$$\frac{-2\pi}{k_0 c} (-\mathrm{j})^m \mathrm{ce_m}(\alpha) \cdot \mathrm{Yc'_m}(0) \cdot D_m = \sum_{n \geqslant 1} Z_0 V_n \cdot Q_{m,n} \left[(1 - \sigma) + \frac{Z_{Teffn}}{Z_r} \right] \tag{76a}$$

and application on both sides of equation (74b) of the integral

$$\int_{-1}^{+1} \cdots \cdot p_{ak}(\xi) \, \mathrm{d}\xi$$

leads to

$$\frac{-N_{ak}}{\Gamma_a Z_a / Z_0} \kappa_k \sin(\kappa_k t) \cdot a_k = \sum_{n \geqslant 1} Z_0 V_n \cdot S_{k,n} \left[(1 - \sigma) + \frac{Z_{Teffn}}{Z_r} \right]. \tag{76b}$$

With $\Delta p = p_e + p_r + p_s - p_a$ inserted into equation (73) and the integral

$$\int_{-1}^{+1} \cdots \cdot v_v(\xi) \, \mathrm{d}\xi, \quad v \geqslant 1,$$

applied on both sides of that equation, one gets

$$Z_{Teffv} N_{pv} \cdot V_v - 4 \sum_{m \geqslant 0} D_m \cdot (-\mathrm{j})^m \mathrm{ce_m}(\alpha) \cdot \mathrm{Hc_m^{(2)}}(0) \cdot Q_{m,v}$$

$$+ \sum_{k \geqslant 0} a_k \cdot S_{k,v} \cdot \cos(\kappa_k t) = 4 P_e \sum_{m \geqslant 0} (-\mathrm{j})^m \mathrm{ce_m}(\alpha) \cdot \mathrm{Jc_m}(0) \cdot Q_{m,v}. \tag{77}$$

One inserts D_m from equation (76a) and a_k from equation (76b) into this equation and finally obtains (an overbar over impedances indicates normalization with Z_0)

$$\sum_{n \geqslant 1} Z_0 V_n \cdot \left[\delta_{n,v} N_{pv} + \frac{2k_0 c}{\pi} \left(\frac{(1-\sigma)}{\bar{Z}_{Teffv}} + \frac{1}{\bar{Z}_r} \right) \sum_{m \geqslant 0} (-\mathrm{j})^m \mathrm{ce_m}(\alpha) \frac{\mathrm{Hc}_\mathrm{m}^{(2)}(0)}{\mathrm{Yc}'_\mathrm{m}(0)} \cdot Q_{m,v} \cdot Q_{m,n} \right.$$

$$\left. - \Gamma_a \bar{Z}_a \left(\frac{(1-\sigma)}{\bar{Z}_{Teffv}} + \frac{1}{\bar{Z}_r} \right) \sum_{k \geqslant 0} \frac{\cot(\kappa_k t)}{\kappa_k \cdot N_{ak}} \cdot S_{k,v} \cdot S_{k,n} \right] = \frac{4P_\mathrm{e}}{\bar{Z}_{Teffv}} \sum_{m \geqslant 0} (-\mathrm{j})^m \mathrm{ce_m}(\alpha) \cdot \mathrm{Jc_m}(0) \cdot Q_{m,v}. \tag{78}$$

This is a linear system of equations ($v = 1, 2, 3 \ldots$) for $Z_0 V_n$. With the solutions, one gets the D_m from equation (76a) and the a_k from equation (76b). If one compares equation (78) with the corresponding system of equations (25) for airtight plates, one sees the transition due to the perforation:

$$\frac{1}{\bar{Z}_{Tv}} \rightarrow \left(\frac{(1-\sigma)}{\bar{Z}_{Teffv}} + \frac{1}{\bar{Z}_r} \right). \tag{79}$$

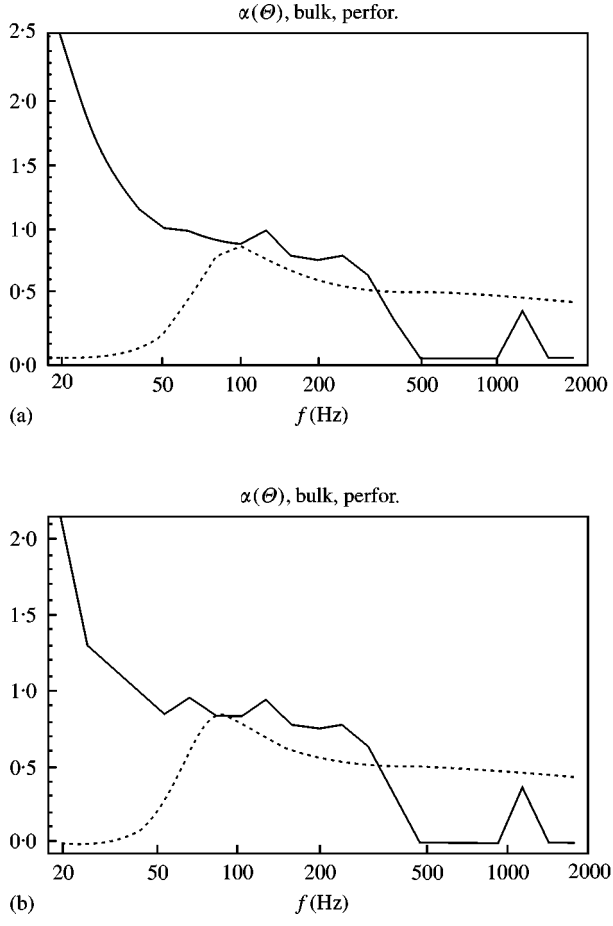

Figure 13. (a) Sound absorption coefficient $\alpha(\Theta)$ for a relatively wide, $c = 0{\cdot}5$ m, porous plywood panel with porosity $\sigma = 0{\cdot}02$ and a high flow resistance $Z_r = 10 \cdot Z_0$ without friction coupling; (dashed: infinite plate); (b) as (a), but with friction coupling; (dashed: infinite plate).

Similar approximations as in section 7 for a tight panel could be derived for a perforated panel also. However, the velocity to be determined is not $V(\xi)$, but $p_{sy}(\xi)$. These approximations are not displayed here in detail.

10. NUMERICAL EXAMPLES WITH PERFORATED PANELS

Only the principal influence of a perforation shall be illustrated. Therefore, the porosity σ and the normalized flow resistance $\mathrm{Re}\{Z_r/Z_0\} = Z_r'/Z_0$ will be entered as new parameters; $\mathrm{Im}\{Z_r/Z_0\}$ (as a consequence of orifice end corrections) will be neglected; this implies either narrow holes in small mutual distances, or Z_r' is increased by an additional resistive sheet. The effect of the porosity on the elastic properties of the panel will be evaluated as described above. The other input parameters will be taken from the examples in section 8, i.e. $\Theta = 45^\circ$; the plywood panel with $d = 6$ mm; $\rho_p = 700\,\mathrm{kg/m^3}$, $f_{cr}d = 20$ Hz m; $\eta = 0{\cdot}02$ and a porosity $\sigma = 0{\cdot}2$; the back volume with $t = 10$ cm is filled with glass fibres with $\Xi = 2500$ Pa s/m^2. The absorption coefficient $\alpha(\Theta)$ evaluated with the analysis of the previous section will be compared with $\alpha(\Theta)$ for an infinite panel; it is evaluated with equations (61) and (62) after the substitution $Z_T \to Z_{Teff}$.

The first examples in Figures 13(a) and 13(b) show the influence of the friction coupling with a relatively wide plate, $c = 0{\cdot}5$ m, and a rather high flow resistance $Z_r = 10 \cdot Z_0$. The effect of friction coupling is high only in a resonance (which is at about 20 Hz in Figure 13(a) and 13(b); it is small for small Z_r (as expected).

The next diagrams are for a similar panel absorber, except that the width is reduced to $c = 0{\cdot}2$; the flow resistance still is $Z_r = 10 \cdot Z_0$. Figure 14(a) is without friction coupling, Figure 14(b) is with friction coupling.

These few examples show that it is possible to construct perforated panel absorbers with interesting low-frequency absorption values by a proper tuning of the parameters.

11. CONCLUDING REMARKS

A rather wide variety of panel absorbers, with airtight or porous panels, and bulk or locally reacting back volumes have been treated with a rigorous field analysis and with some approximations. The high, but narrow resonance peak absorption with airtight panels can be effectively broadened by suitable perforations (no optimization, whatsoever, was intended with the shown examples). Since this type of absorber includes many possible resonance mechanisms, it is advantageous to have a rigorous analysis available. The computing time does not play a decisive role; the shown 3D-plots for the sound fields were evaluated within a few seconds; the diagrams with the absorption coefficient took about 1 min of computation (the times could even be reduced by some integer factor, if the programs would be compiled; uncompiled *Mathematica* programs were used above).

The presented exact analysis may seem to be rather clumsy to some readers. However, one should not forget that one needs an exact analysis for testing more simple approximations, and one should keep in mind that a complicated analysis is no longer an obstacle for practical applications, in times with computers tacting with about 1 GHz, if the analysis is suited for numerical evaluation.

The objects treated in the present paper are two-dimensional (one side of the panel much longer than the other). The question may arise whether a similar analysis can be performed for three-dimensional panel absorbers also (all panel sides finite, and all borders supported).

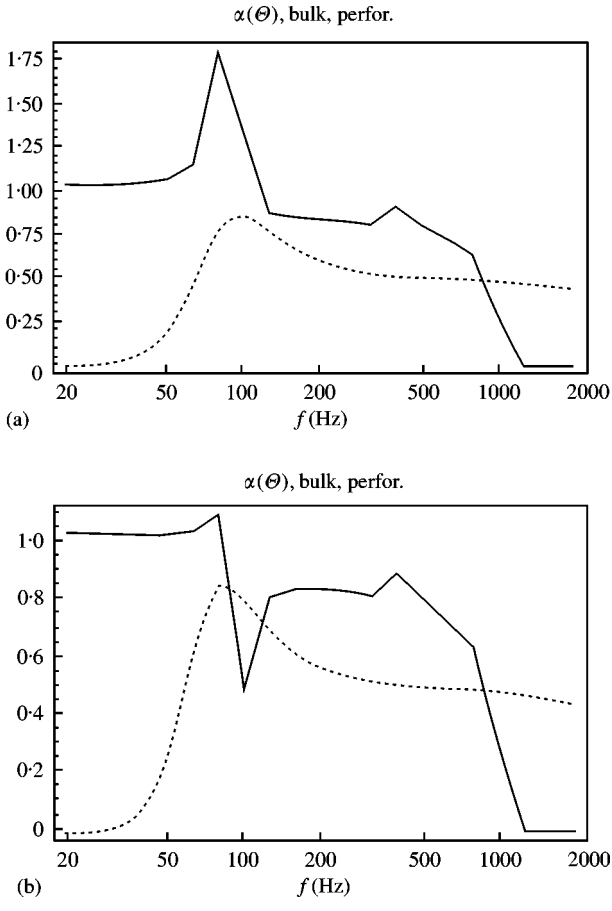

Figure 14. (a) Sound absorption coefficient $\alpha(\Theta)$ for a panel absorber as in Figure 13(a), i.e. without friction coupling, but with a reduced panel width $c = 0{\cdot}2$; (b) sound absorption coefficient $\alpha(\Theta)$ for a panel absorber as in (a) but with friction coupling.

In this context, the role of the elliptic–hyperbolic co-ordinates in the presented exact analysis is recalled, in which the panel and the baffle wall can occupy co-ordinate surfaces, and in which the Helmholtz wave equation can be separated. A similar possibility in three dimensions does not exist for rectangular panels; only circular panels could be treated similarly in spheroidal co-ordinates (the main consequence would be the substitution of Mathieu functions with spheroidal functions). However, one can derive similar approximations as above for three-dimensional absorbers. The presented comparison between the results of exact and approximate solutions in two dimensions suggests that approximations in three dimensions would be acceptable, except in narrow resonances.

REFERENCES

1. L. CREMER and H. A. MÜLLER 1976 *Die wissenschaftlichen Grundlagen der Raumakustik*, Vol. 57, Stuttgart: S. Hirzel Verlag.
2. M. HECKL 1977 *Acustica* **37**, 155–166. Abstrahlung von ebenen Schallquellen.

3. F. P. MECHEL 1989 *Schallabsorber*, Vol. I, Stuttgart: S. Hirzel Verlag; Chapter 8.
4. F. P. MECHEL 1998 *Schallabsorber*, Vol. III, Stuttgart: S. Hirzel Verlag; Chapter 16.
5. F. P. MECHEL 1997 *Mathieu Functions*; *Formulas*, *Generation*, *Use*, Stuttgart: S. Hirzel Verlag.
6. I. S. GRADSTEYN and I. M. RYZHIK. 1980 *Tables of Integrals*, *Series and Products*. New York: Academic Press.
7. F. P. MECHEL 1995 *Schallabsorber*, Vol. II, Stuttgart: S. Hirzel Verlag. Chapter 21–23.